Near Surface Geoscience 2012

C08

Application Results of Compact EM Tool at the Geoelectric Test Site of Institute of Petroleum Geology and Geophysics

E.V. Balkov* (Institute of Petroleum Geology & Geophysics SB RAS)

SUMMARY

A geoelectric prospecting test site was constructed within the area of Kluchi geophysical station (Novosibirsk, IPGG SB RAS). The aim of the test site is to study resolution of the near surface geophysical equipment and to improve methodical base of field works. The ten squares of 100 m2 were used test site design, in which 33 targets simulating various real objects were organized. The following objects were laid down: plastic and metal pipes with different length and diameter, aluminum flasks, plastic jerry cans, etc. In the course of our work the distinctive features of every measured component of the signal were identified. Various targets are identified either in real or imaginary components of the signal. The imaginary component describes the position of the test object more clearly. The phase of signal appears to be an efficient way to display the field data. Targets with different shapes and depths can appear as form of one to five images. It can lead to difficulties connected with the interpretation of this material without prior accumulated methodical information.

Introduction

It is common practice to construct test sites to develop the new instrumental and methodical approaches as well as investigate capabilities of of geophysical equipment. An analysis of the publications and the web content gives an information about several electromagnetic test sites. The first test site "Stanford University Environmental Test Site" is situated in the USA at the Stanford University, second one "UXO Test Site" is presented by Geophex company is located in the North Carolina (USA). The next test site "EIGG Test Site" is located in the Great Britain at the Leicester University. The Moscow State University also organized test site at the Aleksanrovka town. The area of test site is usually splitted to some segments that contain the known targets. According to the published materials the test sites are constructed both by commercial companies and Universities. The companies need it to test and calibrate their equipment while the Universities are used it to make practice for their students. For example, published materials about "Stanford University Environmental Test Site" contain the application results of EM61 equipment [Bosmar, 2001], that realizes shallow TEM approach. The investigation at Geophex test site was made by GEM3 tool [Won et al., 1997], that performs the frequency sounding. The Institute of Petroleum Geology and Geophysics (IPGG SB RAS) organized its own geoelectric test site within the area of Kluchi geophysical station (Novosibirsk, Russia) to test the electromagnetic equipment.

Method and Theory

One of the recent equipment developed by IPGG SB RAS implementing EMI method is NEMFIS (Fig. 1, Manstein et al. 2003, Balkov et al. 2004). Being three coil device with fixed geometry it performs soundings within frequency range from 2.5 to 250 kHz and intended to explore the ground conductivity at the depth up to 10 m. Alternating magnetic field is generated consequently on several (up to 14) fixed frequencies that are chosen to be proportional to the skin depth. Receiver coils are arranged in the transmitter plane lying at straight line (Fig. 1) and those are specifically designed to cancel a primary field. Receivers cancel the primary field in the air by obeying the following relation: $M_1/r_1^3 = M_2/r_2^3$, where M_i and r_i– are moments of the receivers and distances to the transmitter.

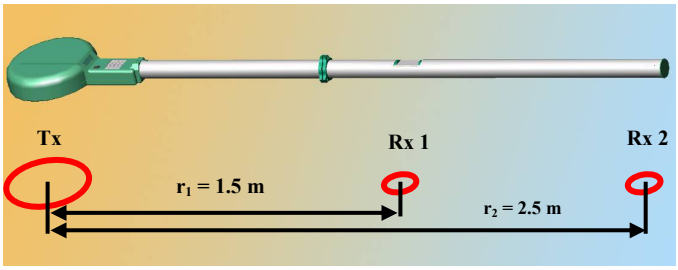

Figure 1 *NEMFIS equipment.*

A model of a homogeneous half space is used to transform soundings (Balkov et al. 2004). The solution of the following transcendental equation yields the apparent value of resistivity (ρ_a):

$$\varepsilon = \varepsilon_1 - \varepsilon_2 = -i\omega\mu \frac{M_T}{2\pi k^2}\left\{\frac{M_1}{r_1^5}\left[9-\left(9+9kr_1+4k^2r_1^2+k^3r_1^3\right)e^{-kr_1}\right]-\right.$$

$$\left.-\frac{M_2}{r_2^5}\left[9-\left(9+9kr_2+4k^2r_2^2+k^3r_2^3\right)e^{-kr_2}\right]\right\},\ k^2 = i\omega\mu_0/\rho_a.$$

Test site description

Before the test site construction the supposed area was studied by NEMFIS tool (fig. 02). Taking into account the mentioned above test sites and the electromagnetic mapping data the new test site was developed. Now it covers 10 squares and contains 33 targets (table below). The size of each square is 10 m by 10 m. There are targets made of different materials are buried at the various depths. The top layer of the area is the soil with the depth up to 1 m. The bottom layer is the water-saturated clay.

Sq. #	*Trgt.#*	Target Description
03	1	Plastic pipe, l = 1.8 m, *D*=110 mm, h = 0.5 m.
03	2	Plastic pipe, l 3.7 m, *D*=60 mm, h = 0.5 m.
03	3	The trench, h = 0.5 m.

06	4	One plastic bottle with the metal chips, V = 5 liters, h = 0.5 m.
06	5	Three plastic bottles with the metal chips, V = 15 liters, h = 0.8 m.
06	6	Metal scrap, V 30x30x30 cm, h = 1.1 m.
06	7	"Anti-aircraft shells ". 2 Metal bars, D = 70 mm, l = 1.1, 0.7 m, h=1.5m
06	8	Aluminum sheet, S = 60x40 cm^2, h = 0.5 m.
06	9	Round Cooper sheet, *D*=0.5 m, h = 0.5 m.
06	10	Round iron sheet, *D*=0.6 m, h = 0.5 m.
08	11	Horizontal iron sheet, S = 1×1.25 m^2. h = 2 m.
08	12	Vertical iron sheet, S = 1×1.25 m^2. h = 1 m (to the top or sheet).
08	13	"Aerial bomb ". Metal pipe with welded sheet. l = 0.85 m. *D*=0.3 m, h= 2 m.
09	14	Metal pipe, l = 4 m, *D* = 100 mm. h = 1 m.
09	15	Metal pipe, l = 5 m, *D* = 100 mm. h = 2 m.
10	16	Dug-out (room S= 2x2 m^2, corridor 1x3 m^2). h = 1m, 2.5 m (to the ceiling, bottom)
11	17	Plastic can (1 pcs.) (V = 35×25×20 cm^3). h = 0.5 m.
11	18	Plastic cans (3 pcs.) (V = 35×25×20 cm^3). h = 1 m.
11	19	Plastic cans (4 pcs.) (V = 35×25×20 cm^3). h = 1.5 m.
12	20	Brick wall. h = 0.5 m, 1.5 m (to the top, bottom).
12	21	Aluminum flask, V = 19 liters, h = 0.5 m (to the top).
12	22	Aluminum flask, V = 19 liters, h = 2.0 m (to the top).
13	23	Iron barrel, V = 200 liters, h = 0.9 m (to the top).
13	24	Iron barrel, V = 200 liters, h = 2.5 m (to the top)
13	25	Iron barrel, V = 200 liters, h = 1.3 m (to the top)
13	26	Iron barrel, V = 200 liters, h = 1.8 m (to the top)
14	27	Horriz. cooper sheet, S = 1x0.6 m^2, h = 0.8 m.
14	28	Vert. cooper sheet, S = 1x0.6 m^2, h = 0.45 m (to the top).
14	29	Horriz. cooper sheet, S = 0.5x0.6 m^2, h = 0.2 m.
14	30	Vert. round iron sheet, *D*=0.6 m, h = 0.5 m.
14	31	Horiz. round iron sheet, *D*=0.6 m, h = 1 m.
15	32	Metal pipe, l = 3 m. *D*=42 mm, h = 0.65 m.
15	33	Metal stick, l = 7.5 m, S = 20×30 mm^2, h = 0.7 m.

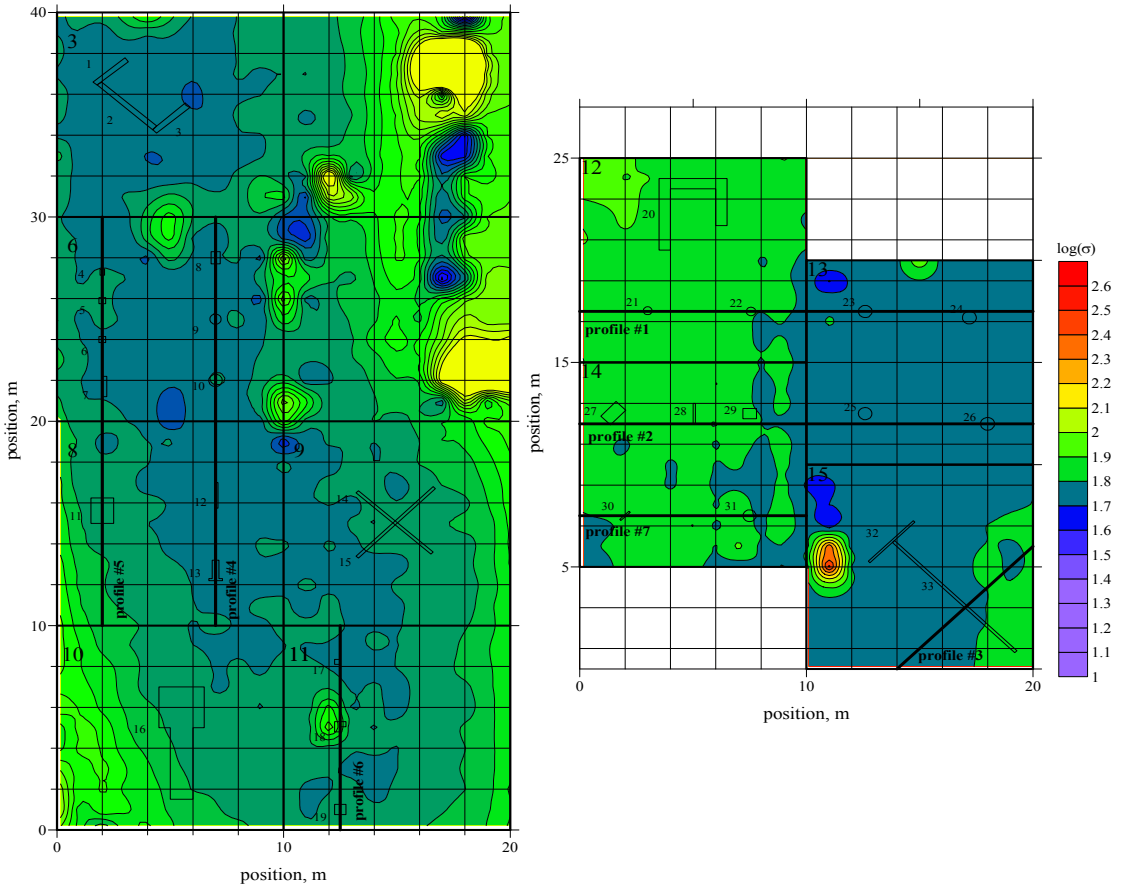

Figure 2 *Test site plan. The maps are results of EMI profiling at 10 kHz frequency.*

Examples

This work contains the results obtained by NEMFIS soundings (2.5 – 250 kHz) at the squares #6,12,14 and along the line #4. The measuring step is the 20 cm. Analysis of results in different components and transformation of the response yield that the phase of response is the most effective value for the detection of local anomalies. Thus all the graphics below contain the images of the phase with all the other components.

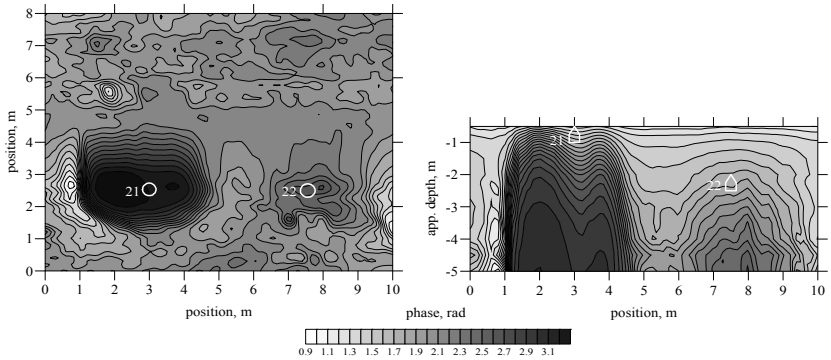

Figure 3 *Map (on the left) and section of distribution of the response phase at the square # 12.*

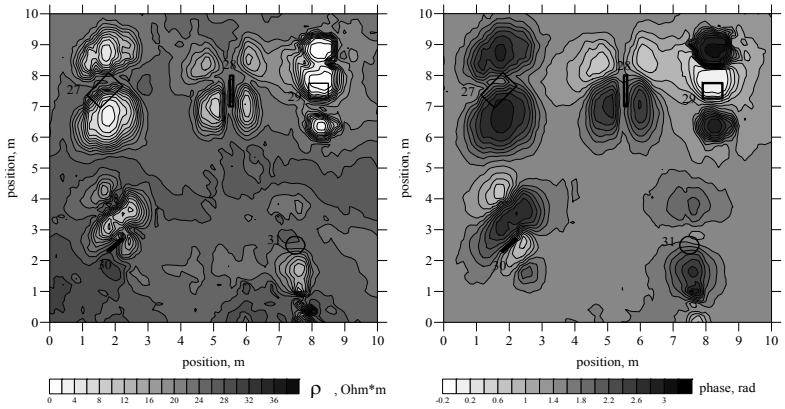

Figure 4 *Apparent resistivity and response phase maps at the square #14 (3.9 kHz).*

The figure 3 shows the map and section of the phase distribution (frequency 10 kHz) on the square #12. The apparent depth on the section is inversely to the square root of the frequency. The frequency of 10 kHz yields the best map, where both the aluminium flask could be seen. It should be noted that the deeper flask (target # 22) is clearly shown only on the phase maps at the low frequencies. The sections demonstrates presence of the both anomalies at the low frequencies.

The maps for the square #14 are the distribution of the apparent resistivity and the phase of response (fig. 4). Both the maps indicates all the targets, that are buried at less than 1 m. Both the visualization yield the clear images but the phase map is more sharp. The NEMFIS tool has three spaced coils thus all the shallow targets produces multiple images. The number of such images is depend on the target depth and form as well as on the profile orientation. It could be seen that horizontal targets (27,29,31) produces two or three anomalies while the vertical targets (28, 30) – four.

Line (profile) #4 crosses five targets on the squares #6 and #8 (see fig. 2). Targets located at the square #8 are buried at the depths 1m (target #12) and 2 m (target #13). Targets located ate square #6 are more shallow. The depth is 0.5 m. Thus the diagrams of various response components (fig. 5) have different intensity. Targets #12 and #13 are clearly seen on the real component diagram, particularly on the high frequencies. Targets #8,9,10 are well indicated for all the components, but the imaginary part of response yields the most clear maximums over these targets at the low frequencies. Both the diagram of absolute response value and imaginary component clearly show only the three shallow targets with the multiple images. The phase diagram indicates all the five targets. The deepest target (#13) there yields minimal anomaly.
Figure 6 shows the map of the real component of response at the frequency of 111 kHz, where all the targets located along the profile #5 are clear indicated. It also demonstrate the pseudo-section along the profile #5.

Conclusion

According to the investigations presented above the following effects could be emphasized. 1. Some targets could be indicated only by real other only by imaginary component of response. The target

position is given more precisely by the imaginary component. 2. The deeper targets could be found by the real component. 3. The diagrams of response phase is yield the most effective visualization of sounding results. Sometimes only the phase indicates the targets. 4. Though the module of response includes both the properties of real and imaginary components its results are least informative. 5. The targets of different shape, depth and orientation could produce from one to four images..

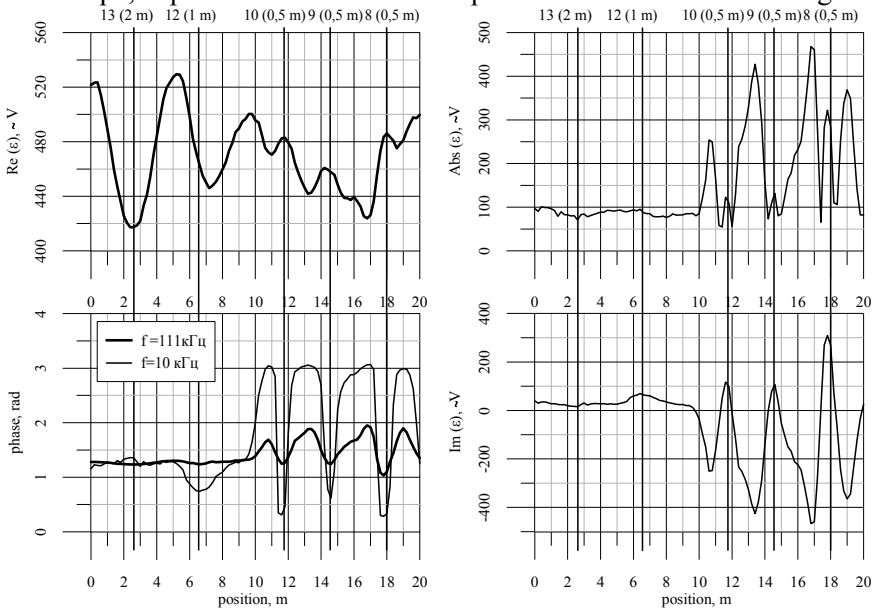

Figure 5 *Diagrams of response along the profile # 4 (freqs. 10 and 110 kHz).*

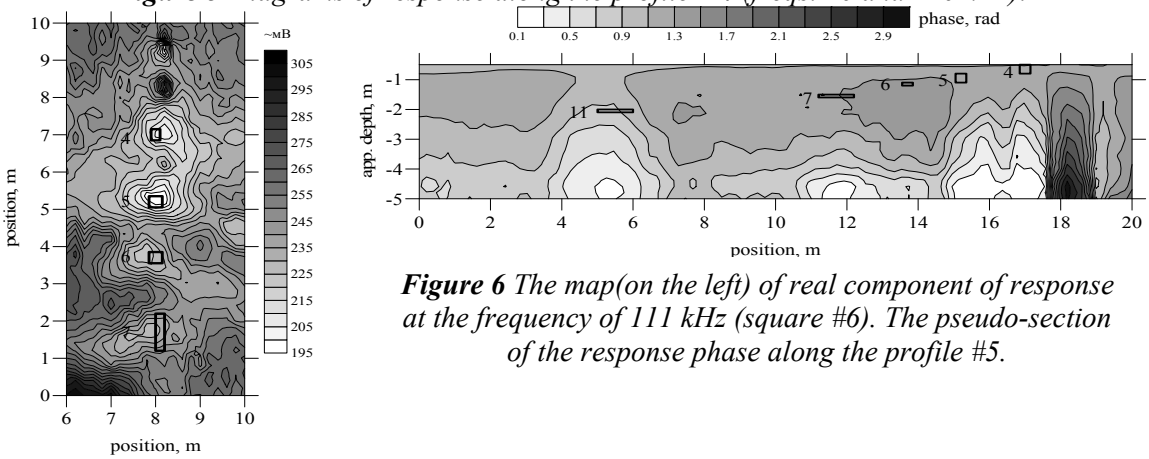

Figure 6 *The map(on the left) of real component of response at the frequency of 111 kHz (square #6). The pseudo-section of the response phase along the profile #5.*

It can be concluded that the proper response interpretation of EMI sensor over the shallow local targets could be made only with prior information and modelling at the test site.

Acknowledgements and References

The research work is performed under support of Presidium of Siberian Branch of Russian Academy of Sciences (grant # 118).

Balkov, E.V., Epov, M.I., Manstein, A.K., Manstein, Y.A. [2004] Elements of Calibration and Data Interpretation of EMI Sounding Device EMS. *Near Surface 2004 Extended Abstracts Book*. 6-9 September, Utrecht, The Netherlands. P-014.

Manstein, A.K., Manstein, Y.A., Balkov, E.V. [2003] EMS Electromagnetic Sounding Device. *9th European Meeting of Environmental and Engineering Geophysics, August 31 – September 4, Prague, Czech Republic*. P-059.

Bosmar M. [2001] Why did Geonics Limited Build the EM61-MK2? Comparison Between EM61-MK2 and EM61. *Geonics Limited Technical Note* TN 33. November.

Won J., Keiswetter D.A., Hanson D.R., Novikova E., Hall T.M. [1997] GEM-3: A monostatic broadband electromagnetic induction sensor. *Journal of Environmental Engineering Geophysics,* **2**, 53-64.